A NEW APPROACH TO MACHINABILITY IN ORTHOGONAL MILLING OF AISI 316L AUSTENITIC STAINLESS STEEL

Óscar Martín, Manuel San-Juan, Pilar De-Tiedra, Francisco Santos

*Universidad de Valladolid, Departamento CMeIM/EGI/ICGF/IM/IPF, Escuela de Ingenierías Industriales, Paseo del Cauce 59, Valladolid 47011, Spain. Tel.: +34 983423533. E-mail: oml@eii.uva.es

Received: 26/Sep/16 -- Accepted: 23/Nov/16 - DOI: http://dx.doi.org/10.6036/8161

ABSTRACT:

Machinability is widely used to compare materials from their ability to give rise to a certain surface finish at the lowest possible tool cost, by using mainly continuous cutting tests such as turning-based tests. Nevertheless, in AISI 316L austenitic stainless steel it is justified to use a broader concept of machinability that also considers the influence of microstructural changes, induced by machining, on the pitting corrosion behaviour.

Keywords: AISI 316L; Machinability; Orthogonal milling; Pitting corrosion.

RESUMEN:

La maquinabilidad es ampliamente utilizada para comparar materiales a partir de su aptitud para dar lugar a un cierto acabado superficial al menor coste de herramienta posible, mediante el uso principalmente de tests de corte continuo tales como los tests basados en torneado. No obstante, en el acero inoxidable austenítico AISI 316L está justificado el uso de un concepto más amplio de maquinabilidad que también considere la influencia de cambios microestructurales, inducidos por el mecanizado, en el comportamiento frente a la corrosión por picaduras.

Palabras clave: AISI 316L; Maquinabilidad; Corte ortogonal; Corrosión por picaduras.

1.- INTRODUCTION

Orthogonal milling is, as reported in [1], a machining process carried out under orthogonal cutting conditions, in which the cutting edge is perpendicular to the cutting speed direction and the process model can be simplified to a two-dimensional model. Traditionally, machinability and standard machining conditions are defined from several specific criteria such as tool wear, machined surface finish, chip removal, cutting rate or productivity, and, according to [2], there are numerous tests that allow performing a benchmarking under this classical acceptation of machinability, although these machinability results may depend on the specific cutting process as pointed out by [3].

Nevertheless, the classical concept of machinability may be broadened by considering other factors such as dimensional accuracy, residual stresses induced by cutting process [4] or surface microstructural changes induced by cutting process and the consequent changes in mechanical and corrosion behaviour, as proposed by [5].

Some authors [6] indicated that austenitic stainless steels, of which the AISI 316L type is an example, are considered difficult to machine due to their high tensile strength, high ductility, high work-hardening and low thermal conductivity; these properties, as pointed out by [7], may give rise to high cutting forces, fast tool wear rates, high susceptibility to notch wear, unstable chip formation, built-up-edge (BUE) formation, poor surface finish and heat concentration in the cutting zone that, in turn, leads to high localized temperatures. These conclusions are based fundamentally on the study of results in continuous cutting conditions and, hence, the study of machinability in orthogonal milling – under non-continuous cutting conditions where the chip thickness is variable – is a significant contribution.

Since, as reported by [8], resistance to corrosion behaviour may be affected by machining and expected pitting corrosion behaviour (PCB) for AISI 316L is good, the possible effect of machining on PCB justifies a broader approach to the concept of machinability.

The present work consists of the following steps: (i) study and measurement of cutting forces; (ii) study of temperature distribution in milling process; (iii) metallographic analysis, justified by the influence of the microstructure on the corrosion behaviour [9]; and (iv) polarization tests: with the aim of studying the effect of the strain induced by

Publicaciones DYNA SL -- c) Mazarredo nº69 - 4º -- 48009-BILBAO (SPAIN)
Tel +34 944 237 566 – www.revistadyna.com - email: dyna@revistadyna.com

orthogonal milling on PCB, *Potentiodynamic Anodic Polarization* (PAP) and *Cyclic Potentiodynamic Polarization* (CPP), which are non-destructive tests widely used to assess the susceptibility of austenitic stainless steels to pitting corrosion [10,11], were performed on the machined samples.

2.- EXPERIMENTAL PROCEDURE

2.1.- MATERIALS

The chemical composition (wt%) of the AISI 316L ASS workpieces was as follows: C, 0.03; Cr, 17.18; Ni, 10.34; Si, 0.036; Mn, 1.35; Mo, 1.86; Al, 0.0193; Co, 0.17; Cu, 0.23; Nb, 0.01; Ti, 0.0212; V, 0.07; W, 0.05; P, 0.031; S, 0.003; Fe, Bal. The workpiece thickness was 5 mm.

2.2.- STUDY OF CUTTING FORCES

End milling tests were performed on workpieces with 200 mm length, 60 mm width and 5 mm thickness, under orthogonal cutting conditions with up-milling configuration, as it is shown in Fig. 1. The workpieces were clamped by using an ad hoc designed system that aimed to reduce the possible effect of the workpiece setting.

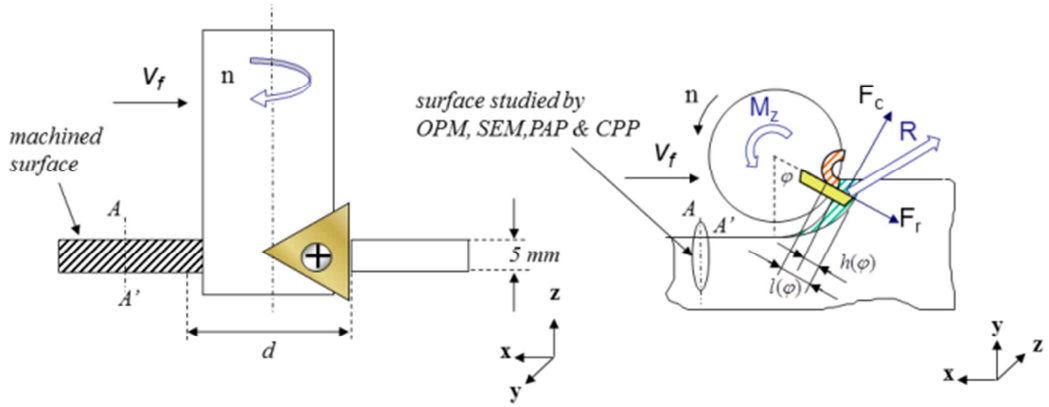

Fig. 1. Orthogonal cutting diagram.

The equipment used to measure cutting forces includes: (i) a Kistler 9124 rotating dynamometer for measuring the three force components associated to a reference system fixed to cutting tool, and (ii) a multichannel portable data acquisition system, 12-bit type WaveBook 512 (IOtech), with a Simultaneous Samples & Hold card, which allows a high speed sampling and which reduces the out-of-phase between acquisition channels. Data processing was carried out by using DasyLabv.8 (National Instruments). The analysis of the axial force F_z allows assessing the correctness of the orthogonal milling hypothesis because the force system can be considered as orthogonal when F_z is lower than 5% of the resultant force R, sum of F_r and F_c.

Since, in the present work, the number of teeth of the milling tool is one, feed per revolution is equal to feed per tooth per revolution ($f=f_t$). Milling tests were carried out with a NC A-16 milling machine and the values of the cutting parameters give rise to eight different samples: (i) sample No. 1: a_p=5 mm, a_e= 3 mm, V= 100 mm/min, f_t= 0.10 mm/rev; (ii) sample No. 2: a_p=5 mm, a_e= 3 mm, V= 100 mm/min, f_t= 0.12 mm/rev; (iii) sample No. 3: a_p=5 mm, a_e= 3 mm, V= 100 mm/min, f_t= 0.15 mm/rev; (iv) sample No. 4: a_p=5 mm, a_e= 3 mm, V= 100 mm/min, f_t= 0.20 mm/rev; (v) sample No. 5: a_p=5 mm, a_e= 3 mm, V= 150 mm/min, f_t= 0.10 mm/rev; (vi) sample No. 6: a_p=5 mm, a_e= 3 mm, V= 150 mm/min, f_t= 0.12 mm/rev; (vii) sample No. 7: a_p=5 mm, a_e= 3 mm, V= 150 mm/min, f_t= 0.15 mm/rev; (viii) sample No. 8: a_p=5 mm, a_e= 3 mm, V= 150 mm/min, f_t= 0.20 mm/rev. Tool diameter was 20 mm, with a TPKN 1603 PPTR-42 IC328 PVD TiCN coated tool insert (ISCAR), and with the following angles: cutting angle 90º, main rake angle 0º, axial rake angle 0º and radial rake angle 0º, for obtaining orthogonal milling conditions. Machining tests were carried out without lubrication and a new cutting edge of the tool insert was used in every test.

Publicaciones DYNA SL -- c) Mazarredo nº69 - 4º -- 48009-BILBAO (SPAIN)
Tel +34 944 237 566 – www.revistadyna.com - email: dyna@revistadyna.com

As indicated in [12], measurement of cutting forces has a high sensitivity to dynamic problems, especially when a rotating dynamometer is used, hence it was necessary to apply a signal filtering to data acquisition (a low-pass filter of 400 Hz was used because the dynamometer/tool system has resonant frequencies around 480 Hz).
Fig. 2 shows the sonogram of the power density spectrum of the resultant force *R* in the working plane: the contribution of different harmonics of the contact frequency between tool and workpiece can be observed. Afterwards, a Buttherworth digital filter was applied, to the signal obtained by the dynamometer, for suppressing the amplification effect in the harmonics of cutting forces by the measuring system resonant frequency.

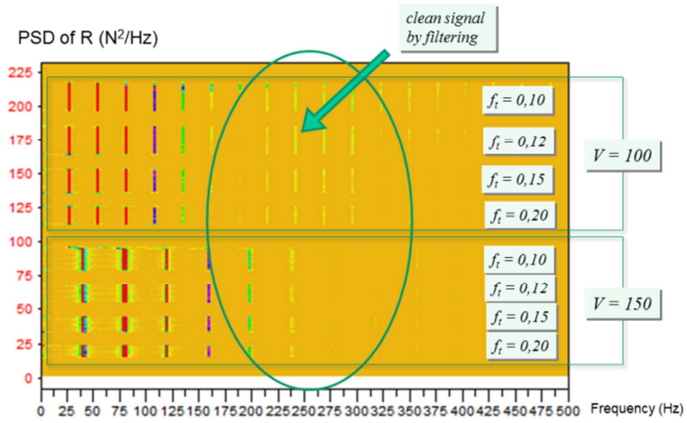

Fig. 2. Sonogram of the power density spectrum of the resultant force R in the working plane. V in m/min and f_t in mm/rev.

2.3.- STUDY OF TEMPERATURES

The experimental methodologies used for assessing the temperature distribution in milling are based on high resolution and high speed thermographic systems of infrared thermography [13,14]. In the present work, an InfraTec ImageIR camera, controlled by with IRBIS 3 Profesional software, was used. Telephoto lenses of 100 mm and 500 mm were used, as done in [15], for achieving high spatial resolution. Given the influence of temperature, surface finish, oxidation or wavelength on emissivity value [16], and with the aim of reducing the uncertainty associated with emissivity characterization, relative or delta measurements of maximum temperature were performed.

2.4.- METALLOGRAPHIC ANALYSIS

The metallographic analysis was performed, using Kalling's reagent, on the surface perpendicular to the machined surface (Fig. 1), by means of optical microscopy (OPM) (Fig. 3a) and scanning electron microscopy (SEM) (Fig. 3b).
Fig. 3 shows a significant presence of strain effects (slip bands) in the area close to the machined surface. Since the slip bands act as preferential sites for pit initiation, as demonstrated in [17], a broader approach to the concept of machinability in ASS, which considers the PCB, may be justified.

Publicaciones DYNA SL -- c) Mazarredo nº69 - 4º -- 48009-BILBAO (SPAIN)
Tel +34 944 237 566 – www.revistadyna.com - email: dyna@revistadyna.com

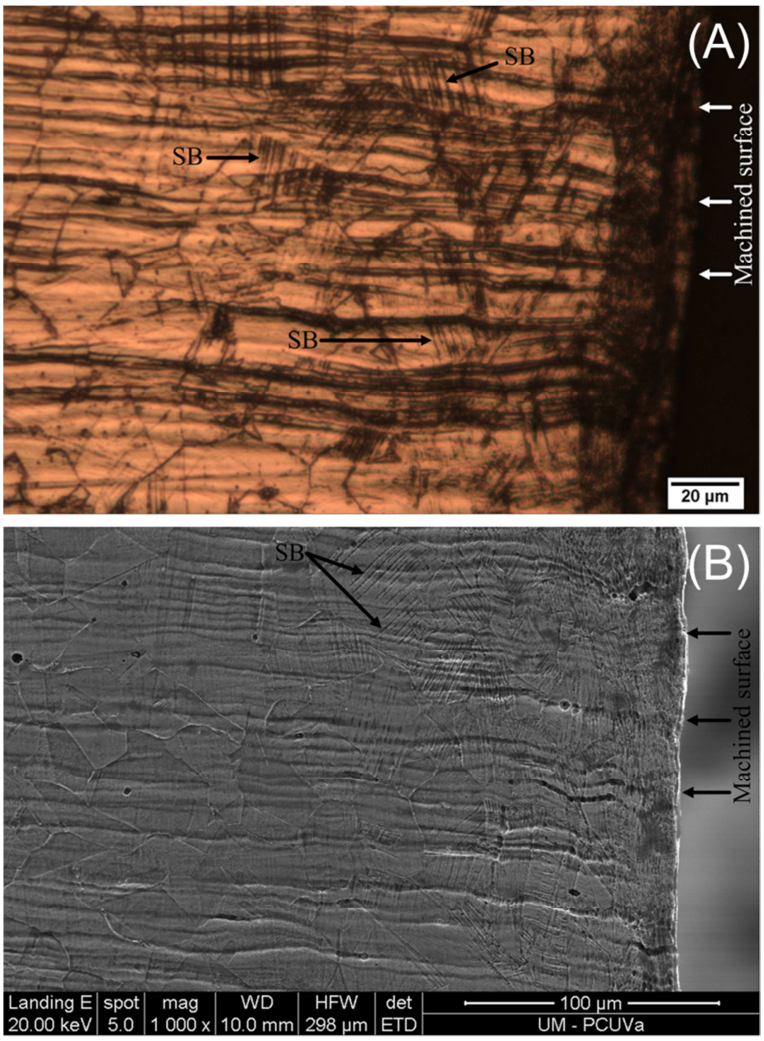

Fig. 3. Micrographs of the surface perpendicular to the machined surface, where the arrows show slip bands (SB), which are strain effects and are located in the area close to the machined surface: (A) OPM, etching with Kalling's reagent, sample No. 8; and (B) SEM, etching with Kalling's reagent, sample No. 4.

2.5.- POLARIZATION TESTS

With the aim of studying the effect of the strain induced by orthogonal milling on PCB, *PAP and CPP* tests were performed on the surface perpendicular to the machined surface.

PAP tests

The PAP tests were carried out according to ASTM G5-94 (Reapproved 1999) [18]. The surface preparation of the specimens was done by polishing up to 1 µm diamond finish. The tests were performed in acid solution with chlorides containing 1 N H_2SO4 + 0.5 N NaCl at a temperature of 30 ºC ± 1. The experimental procedure of the tests was the following: 5 min delay at open circuit potential (V_{OC}), 2 min anodic attack at -220 $mV_{SCE\ (saturated\ calomel\ electrode)}$ [19], then a delay of 2 min at V_{OC}, 2 min cathodic cleaning at -600 mV_{SCE}, 2 min delay at V_{OC} and then anodic potentiodynamic scan that started at 50 mV_{SCE} below V_{OC} until 1000 mV_{SCE}. The potential scan rate was 50 mV/min. PCB was assessed from pitting potential (E_{pit}) parameter obtained from the PAP curve. According to [20,21], the higher the E_{pit}, the higher the pitting resistance.

Publicaciones DYNA SL -- c) Mazarredo nº69 - 4º -- 48009-BILBAO (SPAIN)
Tel +34 944 237 566 – www.revistadyna.com - email: dyna@revistadyna.com

CPP tests

The CPP tests were carried out according to ASTM G61-86 (Reapproved 1998) [22]. The samples were polished up to 1 μm diamond finish. The polarization curves were recorded in 1 N H_2SO_4 + 0.5 N NaCl at a temperature of 30 ºC ± 1. Before polarization the samples were immersed in the test solution for 1 h at V_{OC}. The electrode potential was scanned from V_{OC} at 10 mV/min sweep rate. When the current density reached 5 mA/cm^2 the scanning direction was reversed until V_{OC} to evaluate the repassivation tendency.

Repassivation behaviour was assessed from E_{pit} and repassivation potential (E_{rp}) parameters obtained from the CPP curve. As pointed out in [23], E_{pit}–E_{rp} difference defines the anodic hysteresis loop: the narrower the anodic hysteresis loop, the easier it becomes to repassivate the pit.

3.- RESULTS AND DISCUSSION

The study of cutting forces were performed by using F_c and R. Fig. 4 shows the maximum value, for each turn of the cutting tool, of F_c and R (filtered and non-filtered), as a function of time, for the orthogonal milling conditions used in the present work. As can be seen in Fig. 4, both the maximum values of F_c and R increased with increasing f_t.

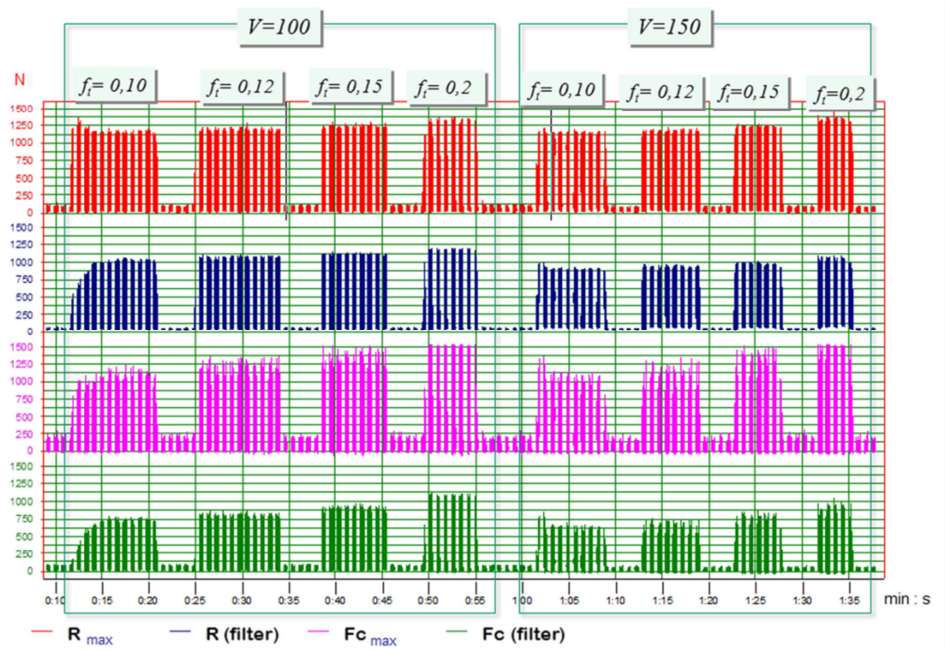

Fig. 4. Maximum value, for each turn of the cutting tool, of F_c and R (filtered and non-filtered), as a function of time. V in m/min and f_t in mm/rev.

A more detailed analysis of F_c and R as a function of time (Figs. 5 and 6), allows observing that: (i) the "cooling time", time between two consecutive maximum force values which allows estimating the available time for heat evacuation, decreased with increasing V (Fig. 5); and (ii) F_c value became closer to that of R with increasing f_t (Fig. 6). These results show that the workpiece temperature tended to decrease with decreasing V and with increasing f_t (as F_c value becomes closer to that of R, F_r and μ decrease).

Publicaciones DYNA SL -- c) Mazarredo nº69 - 4º -- 48009-BILBAO (SPAIN)
Tel +34 944 237 566 – www.revistadyna.com - email: dyna@revistadyna.com

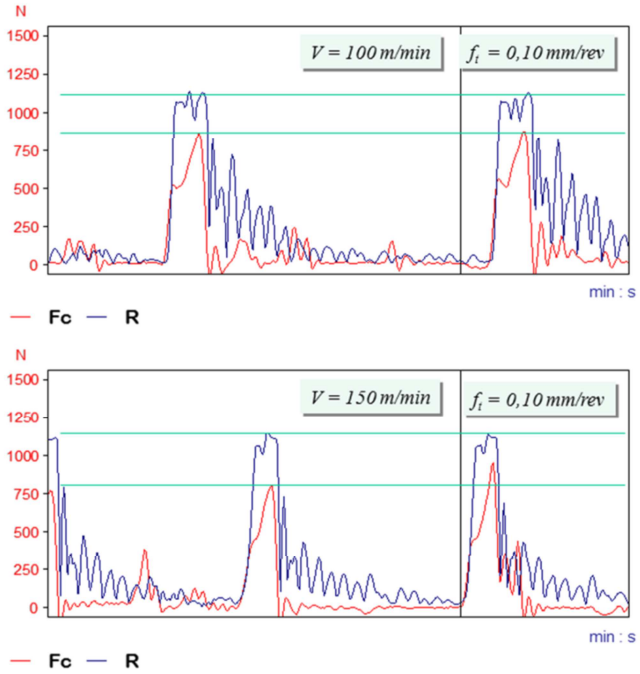

Fig. 5. The "cooling time", time between two consecutive maximum force values which allows estimating the available time for heat evacuation, decreases with increasing V.

The study by using infrared thermography shows that: (i) the highest workpiece temperature was reached in zone 1, where friction prior to chip formation is very high (Fig. 7a); (ii) chip temperature was higher than the highest workpiece temperature; (iii) the increase in cutting speed from V=100 m/min to V=150 m/min led to an increase in the highest workpiece temperature of about 82 ºC (Fig. 7b), this result is consistent with that previously obtained which established that workpiece temperature tends to decrease with decreasing V; and (iv) despite the previous result, which established that workpiece temperature tends to decrease with increasing f_t, there were no significant changes in the highest workpiece temperature by varying f_t.

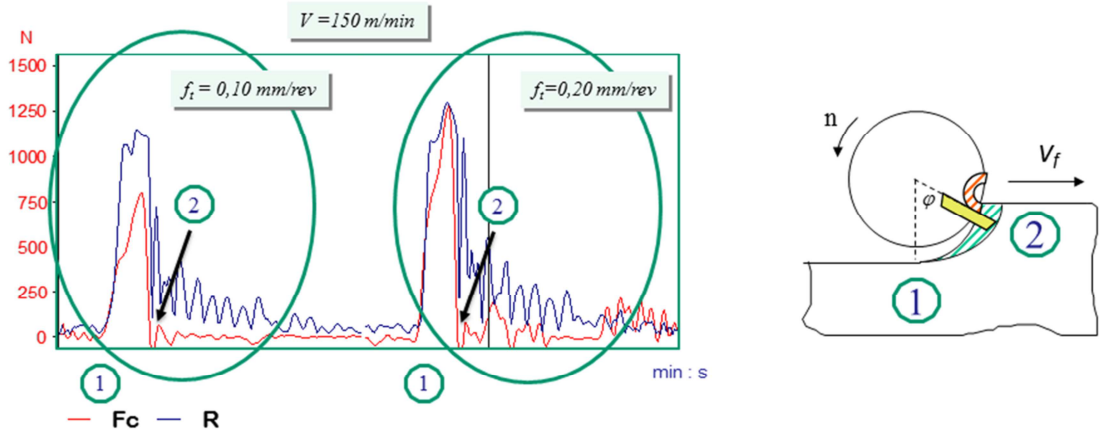

Fig. 6. F_c value becomes closer to that of R with increasing f_t.

Publicaciones DYNA SL -- c) Mazarredo nº69 - 4º -- 48009-BILBAO (SPAIN)
Tel +34 944 237 566 – www.revistadyna.com - email: dyna@revistadyna.com

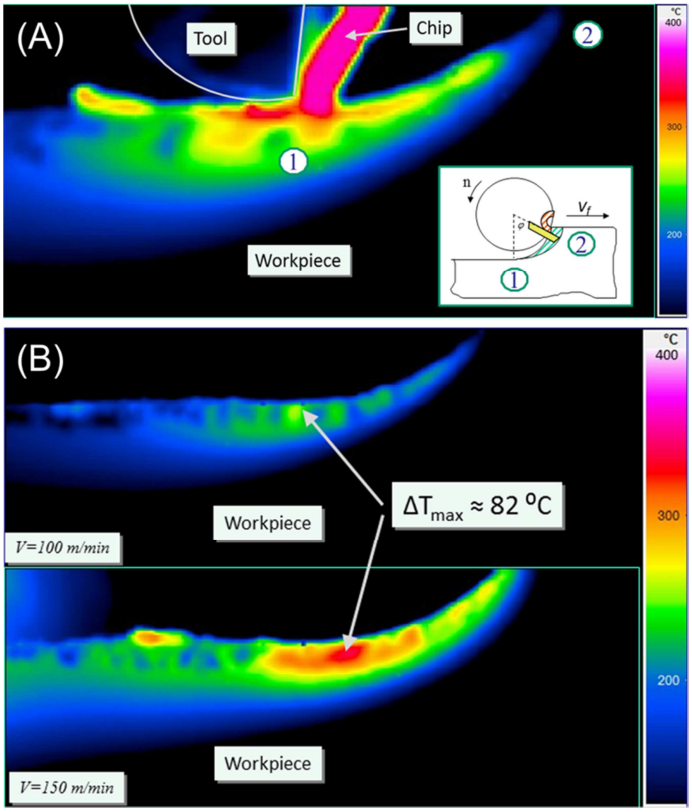

Fig. 7. Infrared thermography image that shows: (A) the workpiece temperatures; and (B) the increase in the highest workpiece temperature (ΔT_{max}) when cutting speed increased from V=100 m/min to V=150 m/min.

PAP curves show that: (i) PCB improved, i.e. E_{pit} increased, with increasing cutting speed V (Fig. 8a); (ii) there were no significant changes in E_{pit} by varying f_t. CPP curves show that: (i) repassivation capacity improved, i.e. E_{pit}–E_{rp} difference decreased, with increasing V (Fig. 8b); and (ii) there were no significant changes in E_{pit}–E_{rp} difference by varying f_t.

The fact that PCB and repassivation capacity improve with increasing V is coherent with the fact that the effects of strain (slip bands), which act as preferential sites for pit initiation, decrease with increasing temperature.

Publicaciones DYNA SL -- c) Mazarredo nº69 - 4º -- 48009-BILBAO (SPAIN)
Tel +34 944 237 566 – www.revistadyna.com - email: dyna@revistadyna.com

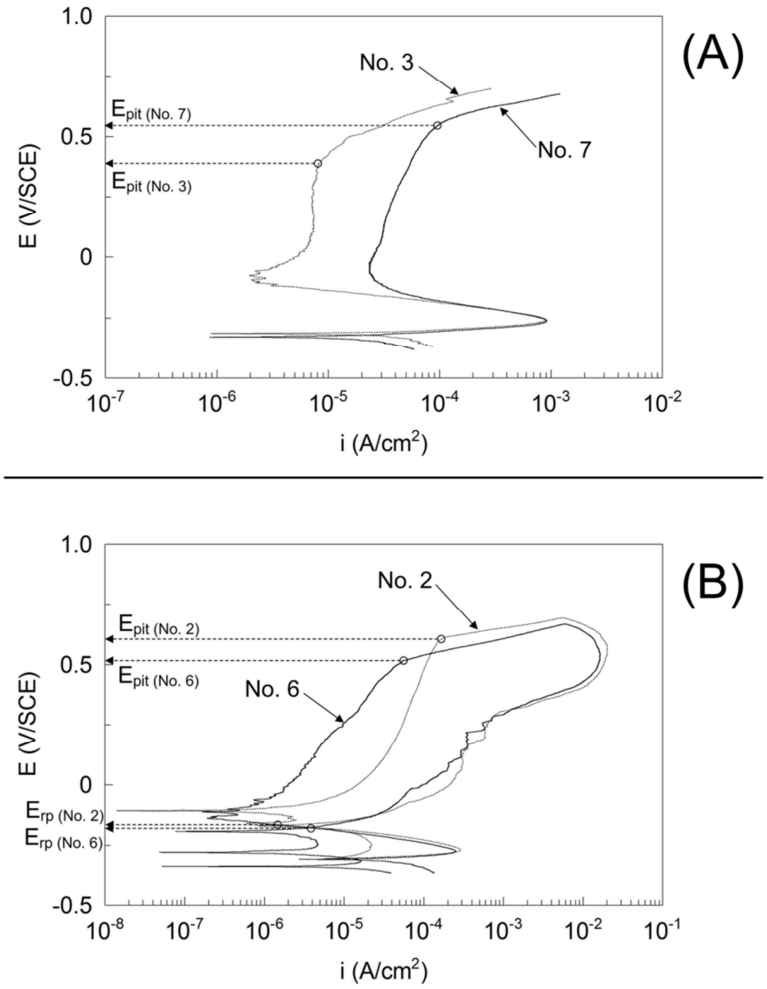

Fig. 8. (A) PAP curves of samples No. 3 (V=100 m/min, f_t=0.15 mm/rev) with E_{pit}=0.41 V and No. 7 (V=150 m/min, f_t=0.15 mm/rev) with E_{pit}=0.56 V. (B) CPP curves of samples No. 2 (V=100 m/min, f_t=0.12 mm/rev) with E_{pit}–E_{rp}=0.77 V and No. 6 (V=150 m/min, f_t=0.12 mm/rev) with E_{pit}–E_{rp}=0.69 V.

4.- CONCLUSIONS

From the present work, the following conclusions can be drawn:

- The analysis of F_c and R forces show that workpiece temperature tended to increase with increasing V: the "cooling time", time between two consecutive maximum force values which allows estimating the available time for heat evacuation, decreased approximately by 33% when V increased from 100 to 150 m/min.
- The study by using infrared thermography shows that the increase in cutting speed from V=100 m/min to V=150 m/min led to an increase in the highest workpiece temperature of about 82 ºC.
- The PAP and CPP curves show that PCB and repassivation capacity improved with increasing V: E_{pit} increased approximately by 37% and E_{pit}–E_{rp} decreased approximately by 10% when V increased from 100 to 150 m/min.
- The analysis of F_c and R forces show that the workpiece temperature tended to decrease with increasing f_t (the ratio R/F_c decreases approximately from 1.5 to 1.0 when f_t increased from 0.10 to 0.20 mm/rev), but there were no significant changes in either the highest workpiece temperature or E_{pit} or E_{pit}–E_{rp} difference by varying f_t.

Publicaciones DYNA SL -- c) Mazarredo nº69 - 4º -- 48009-BILBAO (SPAIN)
Tel +34 944 237 566 – www.revistadyna.com - email: dyna@revistadyna.com

The present work proves the great interest of a broader approach to the concept of machinability of stainless steels, based on the fact that resistance to corrosion behaviour may be affected by machining.

BIBLIOGRAPHY

[1] Ghadbeigi H, Bradbury SR, Pinna C, Yates JR. Determination of micro-scale plastic strain caused by orthogonal cutting. Int J Mach Tools Manuf 2008;48:228–35. doi: http://dx.doi.org 10.1016/j.ijmachtools.2007.08.017.

[2] Bletton O, Duet R, Pedarre P. Influence of oxide nature on the machinability of 316L stainless steels. Wear 1990;139:179–93. doi: http://dx.doi.org 10.1016/0043-1648(90)90044-B.

[3] Santos FJ. Estudio experimental de la fricción en el proceso de corte de un acero AISI 4140 a partir de las fuerzas de corte en el fresado ortogonal. University of Valladolid, 2011.

[4] Valiorgue F, Rech J, Hamdi H, Gilles P, Bergheau JM. A new approach for the modelling of residual stresses induced by turning of 316L. J Mater Process Technol 2007;191:270–3. doi:10.1016/j.jmatprotec.2007.03.021.

[5] Ghosh S, Kain V. Microstructural changes in AISI 304L stainless steel due to surface machining: Effect on its susceptibility to chloride stress corrosion cracking. J Nucl Mater 2010;403:62–7. doi: http://dx.doi.org 10.1016/j.jnucmat.2010.05.028.

[6] M'Saoubi R, Outeiro JC, Changeux B, Lebrun JL, Morão Dias A. Residual stress analysis in orthogonal machining of standard and resulfurized AISI 316L steels. J Mater Process Technol 1999;96:225–33. doi: http://dx.doi.org 10.1016/S0924-0136(99)00359-3.

[7] Maranhão C, Davim JP. Simulation Modelling Practice and Theory Finite element modelling of machining of AISI 316 steel : Numerical simulation and experimental validation. Simul Model Pract Theory 2010;18:139–56. doi:10.1016/j.simpat.2009.10.001.

[8] Thakur A, Gangopadhyay S. State-of-the-art in surface integrity in machining of nickel-based super alloys. Int J Mach Tools Manuf 2016;100:25–54. doi: http://dx.doi.org 10.1016/j.ijmachtools.2015.10.001.

[9] Martín Ó, De Tiedra P, San-Juan M. Study of influence of gamma prime and eta phases on corrosion behaviour of A286 superalloy by using electrochemical potentiokinetic techniques. Mater Des 2015;87:266–71. doi: http://dx.doi.org 10.1016/j.matdes.2015.08.041.

[10] Martín Ó, De Tiedra P, López M. Artificial neural networks for pitting potential prediction of resistance spot welding joints of AISI 304 austenitic stainless steel. Corros Sci 2010;52:2397–402. doi: http://dx.doi.org 10.1016/j.corsci.2010.03.013.

[11] Martín Ó, De Tiedra P, López M, San-Juan M. Combined Effect of Resistance Spot Welding and Post-Welding Sensitization on the Pitting Corrosion Behavior of AISI 304 Stainless Steel. Corrosion 2013;69:268–75. doi: http://dx.doi.org/10.5006/0749.

[12] San-Juan M, Martín Ó, Santos F. Experimental study of friction from cutting forces in orthogonal milling. Int J Mach Tools Manuf 2010;50:591–600. doi: http://dx.doi.org/10.1016/j.ijmachtools.2010.03.013.

[13] Rodríguez Martín M, Lagüela Lopez S, Gonzalez Aguilera D, Diaz Vilariño L. TERMOGRAFÍA ACTIVA, PARTE 1: ENFOQUE TEÓRICO DE LA CAPTACIÓN INFRARROJA, PROCESAMIENTO DE DATOS Y CLASIFICACION. DYNA Ing E Ind 2015;90:456–60. doi: http://dx.doi.org/10.6036/7556.

[14] Rodríguez Martín M, Lagüela Lopez S, Gonzalez Aguilera D, Diaz Vilariño L. TERMOGRAFÍA ACTIVA PARTE 2: DESARROLLO Y APLICACIONES EN INGENIERÍA E INDUSTRIA. DYNA Ing E Ind 2015;90:568–72. doi: http://dx.doi.org/10.6036/7596.

[15] San-Juan M, Santos FJ, De Tiedra P, López R, Martín Ó. APROXIMACIÓN A LA APLICACIÓN DE LA TERMOGRAFÍA IR AL ESTUDIO DEL PROCESO DE FRESADO. DYNA Ing E Ind 2015;90:188–94. doi: http://dx.doi.org/10.6036/7294.

[16] Arrazola PJ, Arriola I, Davies MA. Analysis of the influence of tool type, coatings, and machinability on the thermal fields in orthogonal machining of AISI 4140 steels. CIRP Ann - Manuf Technol 2009;58:85–8. doi: http://dx.doi.org/10.1016/j.cirp.2009.03.085.

[17] Vignal V, Mary N, Valot C, Oltra R, Coudreuse L. Influence of Elastic Deformation on Initiation of Pits on Duplex Stainless Steels. Electrochem Solid-State Lett 2004;7:C39. doi: http://dx.doi.org/10.1149/1.1647995.

[18] ASTM G5-94 (Reapproved 1999). Standard reference test method for making potentiostatic and potentiodynamic anodic polarization measurements. 1999.

[19] Park I-J, Lee S-M, Kang M, Lee S, Lee Y-K. Pitting corrosion behavior in advanced high strength steels. J Alloys Compd 2015;619:205–10. doi: http://dx.doi.org/10.1016/j.jallcom.2014.08.243.

[20] Li HB, Jiang ZH, Feng H, Zhang SC, Li L, Han PD, et al. Microstructure, mechanical and corrosion properties of friction stir welded high nitrogen nickel-free austenitic stainless steel. Mater Des 2015;84:291–9. doi: http://dx.doi.org/10.1016/j.matdes.2015.06.103.

[21] De Tiedra P, Martín Ó, San-Juan M. Potentiodynamic study of the influence of gamma prime and eta phases on pitting corrosion of A286 superalloy. J Alloys Compd 2016;673:231–6. doi: http://dx.doi.org/10.1016/j.jallcom.2016.02.261.

[22] ASTM G61-86 (Reapproved 1998). Standard test method for conducting cyclic potentiodynamic polarization measurements for localized corrosion susceptibility of iron-, nickel-, or cobalt- based alloys. 1998.

[23] AghaAli I, Farzam M, Golozar MA, Danaee I. The effect of repeated repair welding on mechanical and corrosion properties of stainless steel 316L. Mater Des 2014;54:331–41. doi: http://dx.doi.org/10.1016/j.matdes.2013.08.052.

Nomenclature

a_p axial cutting depth (mm)

a_e radial cutting depth (mm)

Publicaciones DYNA SL -- c) Mazarredo nº69 - 4º -- 48009-BILBAO (SPAIN)
Tel +34 944 237 566 – www.revistadyna.com - email: dyna@revistadyna.com

F_c	cutting force (N)
F_r	radial force (N)
F_z	axial force (N)
R	resultant force (N)
f	feed per revolution (mm/rev)
f_t	feed per tooth per revolution (mm/rev)
h	chip thickness (mm)
l	tool-chip contact length (mm)
V	cutting speed (m/min)
v_f	feed rate (mm/min)
φ	angular position of the tooth (deg)
μ	friction coefficient
E_{pit}	pitting potential (V)
E_{rp}	repassivation potential (V)

Publicaciones DYNA SL -- c) Mazarredo nº69 - 4º -- 48009-BILBAO (SPAIN)
Tel +34 944 237 566 – www.revistadyna.com - email: dyna@revistadyna.com